8

Trace gas measurements using cavity ring-down spectroscopy

Shui-Ming Hu

HEFEI NATIONAL LABORATORY FOR PHYSICAL SCIENCES AT MICROSCALE, CAS CENTER FOR EXCELLENCE AND SYNERGETIC INNOVATION CENTER IN QUANTUM INFORMATION AND QUANTUM PHYSICS, UNIVERSITY OF SCIENCE AND TECHNOLOGY OF CHINA, HEFEI, ANHUI PROVINCE, CHINA

8.1 Introduction

The sensitivity of conventional direct absorption spectroscopy in detecting trace gases is primarily limited by the effective absorption path length and the power noise of the light source. A common method of increasing the effective path length is to use a multipass absorption sample cell. To avoid interference of the beam overlapping in the cell, it is generally required to use large-size mirrors, which eventually leads to an increase in the volume of the sample cell. Amplitude or wavelength (frequency) modulation of the incident light can be used to suppress the power noise of the light source. Usually, these methods can enhance the sensitivity by approximately two to three orders of magnitude but the sensitivity is still insufficient for many applications.

The effective absorption path length can be greatly enhanced by using a resonant cavity. Kastler and Alfred first demonstrated that the intensity of light transmitted from an optical cavity is exponentially attenuated (Kastler, 1974). Later Anderson et al. used the technique to determine the reflectivity of high-reflective (HR) mirrors by measuring the ring-down time of a He−Ne laser beam passing through an optical cavity (Anderson et al., 1984). In 1988, O'Keefe and Deacon built the first cavity ring-down spectroscopy (CRDS) device using a pulsed laser, and successfully measured the spectrum of the oxygen molecule, marking the beginning of the CRDS technology (O'Keefe and Deacon, 1988). In the CRDS measurement, on the one hand, the use of resonant cavity considerably increases the effective absorption path length, and on the other hand, the measured signal decay rate is independent of the initial intensity of the laser, thereby suppressing the noise due to fluctuations in the laser power. Therefore, the sensitivity is improved significantly. Since the optical beams completely overlap in the cavity, a reduced sample volume is feasible compared with conventional multipass configurations (White−or Herriot-type) where relatively large mirrors are needed to separate

Advances in Spectroscopic Monitoring of the Atmosphere. https://doi.org/10.1016/B978-0-12-815014-6.00002-6

different passes of light. As a direct absorption spectroscopy method, compared with mass spectrometry, chromatography, and other technologies, CRDS has an important advantage that the content or concentration of the target molecule can be directly obtained. The technology has been used in various applications to detect molecules in gas phase, such as chemical dynamics studies (Berden et al., 2000; Brown, 2003), explosives detection (Taha et al., 2013), environmental pollutant monitoring, and disease marker diagnostics (Wang and Sahay, 2009; Henderson et al., 2018).

The techniques and applications of CRDS have been reviewed in quite a few references, including the book edited by Berden and Engeln (2009). Here we will concentrate on the fundamental methods of CRDS and its application in trace gas analysis. An introduction of the experimental method of CRDS, including the principle, implementation, and performance will be presented in Section 2. A review of applications in trace gas detection using CRDS, in terms of the operation wavelength and the limit of detection (LOD) for different molecules, will be given in Section 3. A brief summary is given in the last section.

8.2 Experimental methods of CRDS

8.2.1 Principles of CRDS

The configuration of a typical CRDS instrument is shown in Fig. 8.1(a). A laser beam is coupled into an optical cavity and the transmitted light is detected by a photodetector (PD) and recorded by a data acquisition device. Fig. 8.1(b) illustrates the process to produce a ring-down event. When incident light is switched off, light transmitted from the optical cavity decays exponentially. By measuring the decay rate of this signal, one

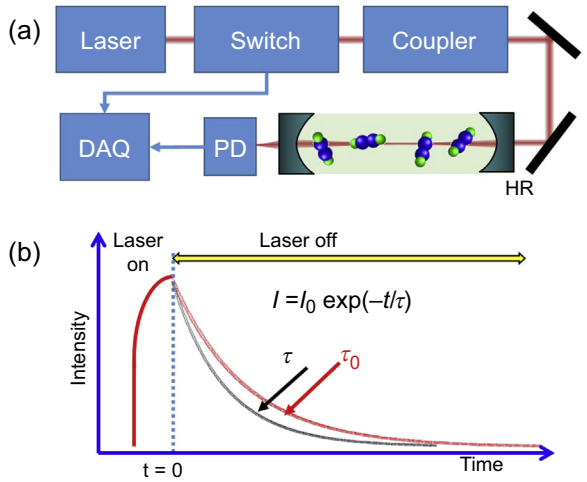

FIGURE 8.1 (a) Configuration of cavity ring-down spectroscopy. *DAQ*, data acquisition system; *HR*, high-reflective mirror; *PD*, photodetector. (b) Signal of ring-down events with and without sample.

can get the corresponding ring-down time, which is related to the loss of the light traveling in the optical cavity. The absorption coefficient of the sample in the cavity can be determined from the change of the ring-down time:

$$\alpha = \frac{1}{c\tau} - \frac{1}{c\tau_0} \tag{8.1}$$

where c is the speed of light, τ and τ_0 are ring-down times with and without sample in the cavity, respectively. For a cavity consisting of two identical HR mirrors, the decay rate of the empty cavity is

$$\frac{1}{c\tau_0} = \frac{1-R}{L} \tag{8.2}$$

where L is the cavity length and R is the reflectivity of the HR mirror. When using a mirror with a reflectivity $R > 99.9\%$, the cavity's ring-down time is generally in the range of a few microseconds to hundreds of microseconds. The effective absorption path length $\left(\approx \frac{L}{1-R}\right)$ easily reaches tens of kilometers. Since the decay rate of the light intensity is measured, regardless of the initial intensity of the incident light, CRDS is naturally immune to the power noise of the laser. As a result, the detection sensitivity is considerably improved.

8.2.2 Optical resonant cavity

CRDS is basically one of the cavity-enhance absorption spectroscopy methods. First we give a brief introduction to the properties of passive optical resonant cavities. More comprehensive explanation can be found in the literature (Zalicki and Zare, 1995; Lehmann and Romanini, 1996; Hodges et al., 1996; Born and Wolf, 1999; Berden and Engeln, 2009).

For simplicity, we assume the incident laser has an ideal Gaussian profile. In order to achieve a stable optical cavity, it is required that the Gaussian beam is reflected back and forth in the cavity, and remains in the cavity with minimal leakage. If the radii of curvature of the two HR mirrors constituting the cavity are r_1 and r_2, respectively, with a cavity length of L, the stable cavity condition is

$$\begin{aligned} g_1 &= 1 - \frac{L}{r_1} \\ g_2 &= 1 - \frac{L}{r_2} \\ 0 &< g_1\ g_2 < 1 \end{aligned} \tag{8.3}$$

where g_1 and g_2 are corresponding geometrical factors. If two identical mirrors are used, the stable cavity condition is $L < 2r$. Note that we get a confocal cavity when $r_1 = r_2 = L$.

In a stable cavity, the waist of the Gaussian beam, defined as the diameter of the beam when the intensity drops to $1/e^2$ of the maximum, can be derived as follows:

$$\omega_0^2 = \frac{L\lambda}{\pi}\sqrt{\frac{g_1 g_2(1-g_1 g_2)}{(g_1+g_2-2g_1 g_2)^2}} \tag{8.4}$$

where λ is the wavelength of the laser light. The distances from the waist to two HR mirrors are

$$\begin{aligned} z_1 &= \frac{g_2(1-g_1)}{g_1+g_2-2g_1 g_2}\boldsymbol{L} \\ z_2 &= \frac{g_2(1-g_2)}{g_1+g_2-2g_1 g_2}\boldsymbol{L} \end{aligned} \tag{8.5}$$

and the beam size at the first HR mirror is

$$\omega_1^2 = \frac{L\lambda}{\pi}\sqrt{\frac{g_2}{g_1(1-g_1 g_2)}} \tag{8.6}$$

When a single-frequency laser beam transmits through the cavity, the transmittance depends on the laser frequency and the cavity parameters, which can be described by a periodic Airy function, as illustrated in Fig. 8.2. When R is close to 1, the peaks get very narrow and their positions are called the (longitudinal) modes of the cavity. The frequency interval between two adjacent cavity modes is called the free spectral range (FSR) of the cavity:

$$\mathrm{FSR} = \nu(q+1) - \nu(q) \approx \frac{c}{2nL} \tag{8.7}$$

where n is the refractive index of the gas inside the cavity, c is the speed of light, and q is the mode index. Note that the FSR value may vary slightly with q due to dispersion of the mirror coating.

The finesse of the cavity is defined as the ratio between FSR and the width δf (full width at half maximum) of a longitudinal mode:

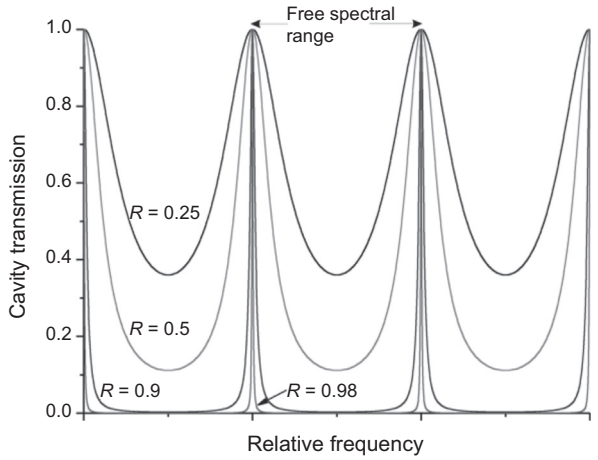

FIGURE 8.2 Transmission of an optical cavity composed of two mirrors with a reflectivity of ***R***.

$$\mathrm{F}=\frac{\mathrm{FSR}}{\delta f}=\frac{\pi\sqrt{R}}{1-R}. \tag{8.8}$$

For a 1-m-long cavity consisting of a pair of mirrors with a reflectivity of 99.99% (F = 30,000), the empty cavity has an FSR of 150 MHz (0.005 cm^{-1}), and the width of a cavity mode is only 5 kHz which is much narrower than linewidths of most commercial lasers.

When the incident laser frequency is on resonance with a cavity mode, part of the laser beam will pass through the cavity and transmit from the other end of the cavity. The reflectivity of the cavity is (Ma et al., 1999; Wang et al., 2017b)

$$R=\frac{P_r}{P_{in}}=\left(\frac{(t_2-t_1+\ell_1+\ell_2+2\alpha L)}{(t_2+t_1+\ell_1+\ell_2+2\alpha L)}\right)^2, \tag{8.9}$$

the transmittance is

$$T=\frac{P_t}{P_{in}}=\frac{4t_2t_1}{(t_2+t_1+\ell_1+\ell_2+2\alpha L)^2}, \tag{8.10}$$

and the laser field inside the cavity will be considerably enhanced by a factor

$$\varepsilon=\frac{P_c}{P_{in}}=\frac{4t_1}{(t_2+t_1+\ell_1+\ell_2+2\alpha L)^2}, \tag{8.11}$$

Here P_{in} is the power of the incident laser before the first HR mirror, P_r is the reflected power at the first HR mirror, P_t is the power transmitted from the cavity (after the second HR mirror), and P_c is the power inside the cavity. Factors t_1, t_2 are the transmittance coefficients of the first and second HR mirrors, l_1, l_2 are the loss coefficients, and αL is the single-path loss due to the absorption and scattering of the sample inside the cavity.

The Gaussian beam also propagates laterally within the cavity, resulting in the appearance of transverse modes. Each transverse mode has a diffraction loss in the cavity and results in a decrease in laser power. The lowest order transverse mode TEM_{00} usually has the smallest diffraction loss, therefore one needs to suppress high-order transverse modes in the optical design, increasing the TEM_{00} signal in the measurement.

In paraxial conditions, Gaussian beams are usually described with a complex parameter q:

$$\frac{1}{q(z)}=\frac{1}{R(z)}-i\frac{\lambda}{\pi w^2(z)} \tag{8.12}$$

where z is the distance to the waist of the Gaussian beam, $R(z)$ is the radius of curvature of the isophase plane of the Gaussian beam, and $w(z)$ is the radius of the beam at z. They follow the equations:

$$\begin{aligned} z_0&=\frac{\pi w_0^2}{\lambda}\\ w^2(z)&=w_0^2\left(1+\frac{z^2}{z_0^2}\right)\\ R(z)&=z\left(1+\frac{z_0^2}{z^2}\right) \end{aligned} \tag{8.13}$$

The propagation characteristics of a Gaussian beam in an optical component can be described by the "ABCD" law:

$$q' = \frac{Aq + B}{Cq + D} \tag{8.14}$$

where A, B, C, D are elements in the transfer matrix $\begin{pmatrix} A & B \\ C & D \end{pmatrix}$. Different optical components have different matrix elements, some common ones are as follows:

(1) free space propagation for a distance d in a medium of refractive index n: $\begin{pmatrix} 1 & \frac{d}{n} \\ 0 & 1 \end{pmatrix}$;

(2) at the plane from the medium of refractive index n_1 to the medium of refractive index n_2: $\begin{pmatrix} 1 & 0 \\ 0 & \frac{n_1}{n_2} \end{pmatrix}$;

(3) at the spherical surface of radius r from the medium of refractive index n_1 to the medium of refractive index n_2: $\begin{pmatrix} 1 & 0 \\ \frac{n_2 - n_1}{n_2 r} & \frac{n_1}{n_2} \end{pmatrix}$.

In the experiment, one can first measure the beam waist radius of the Gaussian beam using a beam analyzer, and calculate the beam waist and position in the cavity using the ABCD matrix. Then by selecting lenses of different focal lengths and adjusting the distances, one can make the TEM_{00} beam coincide with the previously calculated one. If the incident light frequency also resonates with the cavity mode, it will be possible to couple the incident light into the optical cavity with a high efficiency.

8.2.3 Cavity mode match and frequency calibration

If a pulsed laser is used as the light source in CRDS, laser pulses with a duration of a few nanoseconds or shorter have a linewidth (in the frequency domain) broader than the FSR of the cavity, and can be directly coupled into the cavity to produce ring-down events. However, in each ring-down event, multiple longitudinal modes of the optical cavity with different frequencies are simultaneously excited, which limit the frequency resolution of the spectrometer. In addition, the pulsed laser may also excite multiple transverse modes in the optical cavity. The interference among all the excited modes also causes fluctuation in the transmitted light signal, thereby reducing the sensitivity of the spectrometer. Fig. 8.3(a) shows an example of the recorded ring-down curve when two modes in the cavity were excited: one is the TEM_{00} mode and the other one is a high-order transverse mode. Clear pattern of beating can be observed in the recorded curve.

Romanini et al. (1995) proposed an idea of implementing CRDS using continuous-wave (cw) lasers. On the one hand, the use of a narrow-linewidth cw laser as the light

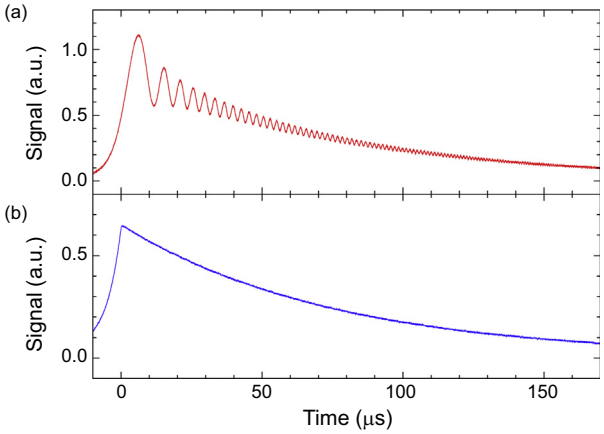

FIGURE 8.3 Ring-down curve when multiple cavity modes are excited (a) and that when only one cavity mode is excited (b).

source greatly increases the frequency resolution, which makes it possible for precision spectroscopy. On the other hand, since only one transverse mode is excited in each ring-down event, the interference effect is eliminated, and the detection sensitivity can also be greatly improved. As a comparison, Fig. 8.3(b) shows a ring-down curve when only the TEM_{00} mode of the cavity was excited.

The main difficulty in using a single-frequency cw laser as the light source is to achieve a frequency match between the laser and the longitudinal mode of the ring-down cavity. Since the finesse of the cavity can be as high as 10,000 or more, the width of a cavity mode is 10 kHz or narrower. Fig. 8.4 illustrates longitudinal modes of an optical cavity. Fig. 8.4(b) was obtained by locking the laser onto one longitudinal mode, passing another laser beam with an adjustable frequency shift through the empty cavity, and measuring its transmitted power. Note that when the cavity is filled with sample gas, the frequencies of the cavity modes also change due to the change of the refractive index. Moreover, as shown in Fig. 8.4(c), the transmittance of the cavity decreases and the width of the mode increases in the vicinity of the molecular absorption line. Note that frequency distances between nearby modes are also changed due to the dispersion effect of the absorption line, and this effect can be applied to detect gas by measuring the frequency shifts of the cavity modes (Cygan et al., 2015; Kang et al., 2018a).

There are two methods in general to match the laser frequency with the cavity. One is referred to the "dither-mirror" mode, which is by scanning the cavity length to match a fixed laser wavelength. The method was first implemented by Romanini et al. (1997a,b,c), and later became the most popular way of cw-CRDS applied in many groups (Brown, 2003; Morville et al., 2004; Paldus and Kachanov, 2005; Huang and Lehmann, 2007; Gao et al., 2010; Pan et al., 2011). A common applied approach of this method is shown in Fig. 8.5. A triangle wave was used to drive a piezo actuator (PZT) attached to one HR mirror to quickly dither the HR mirror. When the frequency of a longitudinal

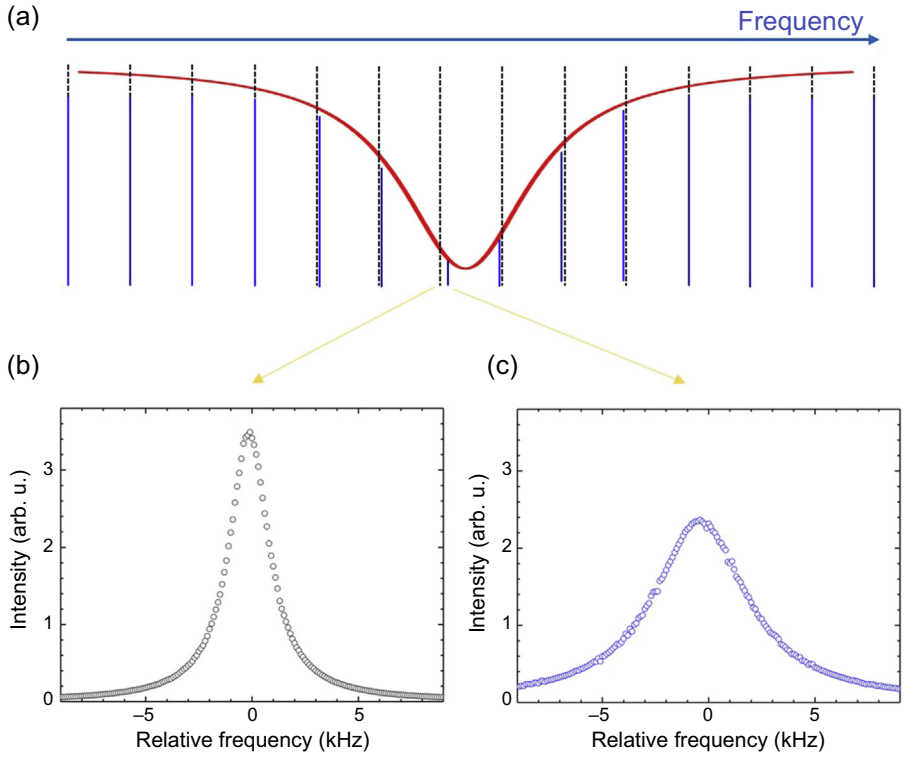

FIGURE 8.4 Transmittance spectrum of a high-finesse cavity. (a) Dash lines indicate the longitudinal modes of an empty cavity, and the solid lines present the modes when the cavity is filled with gas and an absorption line is located in this spectral range. Note that the mode frequencies are shifted, but the shifts were exaggerated for better illustration. (b) Transmittance spectrum around a cavity mode of an empty cavity. (c) Transmittance spectrum around a cavity mode close to the center of the molecular absorption line. Note the height of the mode considerably decreases but the width increases.

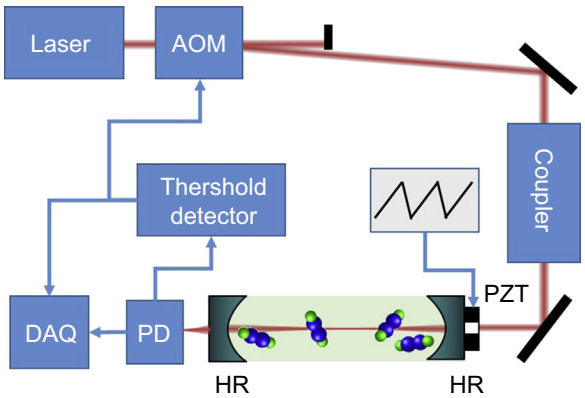

FIGURE 8.5 Simplified scheme of the cw-CRDS setup using the "dither-mirror" method.

mode of the cavity matches the laser frequency, the laser beam starts to enter the cavity and builds up the field inside the cavity. When the intensity reaches a preset level, an acousto-optic modulation (AOM) will be triggered to turn off the laser, which initiates a ring-down event. The light transmitted from the cavity will be recorded and digitized, and a program will be used to fit the data with an exponential function to derive the ring-down time.

In this "dither-mirror" mode, the laser wavelength needs to be calibrated separately, such as by using an étalon or a wavemeter. Pan et al. (2011) locked the laser on a stable cavity made of low-expansion material, and then used an electro-optic modulator (EOM) to generate a sideband for CRDS detection. The spectral scan was accomplished by changing the radiofrequency driving the EOM, therefore the precision could be easily improved to the sub-MHz level. More accurate frequency calibration requires the use of an ultrastable reference laser or an optical frequency comb, or directly locking the probe laser frequency to the comb. Note that the cavity mirror is vibrating in this method, which produces a Doppler shift of the frequency of the light field inside the cavity from that of the incident laser. The effective frequency shift is proportional to the speed of the mirror multiplied by the finesse of the cavity (Lee and Hahn, 2004), and the typical value is hundreds of kHz or even a few MHz, which may limit the frequency accuracy of measurements using the "dither-mirror" method.

An alternative method, referred to as the "dither-laser" mode below, is to quickly dither the laser frequency without changing the cavity length (Schulz and Simpson, 1998; van Leeuwen et al., 2003; Orr and He, 2011). As shown in Fig. 8.6, when the laser scans to the frequency matching a cavity mode, the laser enters the cavity. An advantage of this method is that the FSR of the cavity can be used as a reference for calibrating the laser

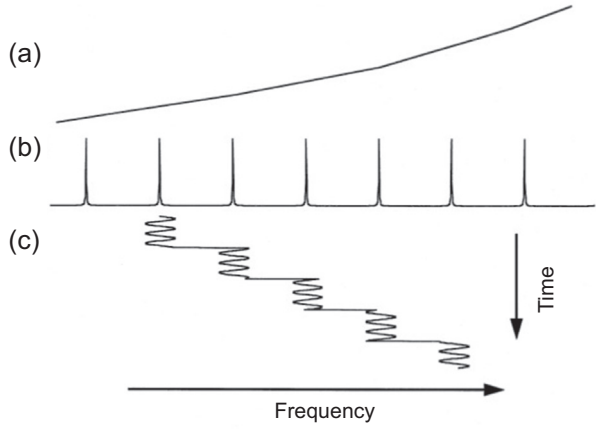

FIGURE 8.6 CRDS scan pattern of the "scanning laser" mode, matching the laser frequency to the cavity modes. Line "a" represents a slowly varying absorption cross section versus light frequency. Ring-down transients are recorded at each étalon transmission peak, shown as line "b." Line "c" shows the laser scan pattern with time increasing downward. *Figure reprinted with permission from Schulz, K.J., Simpson, W.R., 1998. Frequency-matched cavity ring-down spectroscopy. Chem. Phys. Lett. 297, 523–529. Copyright 1998 Elsevier.*

frequency, if the cavity length is sufficiently stable during the measurement. Note that only relative frequencies are calibrated in this way, and a limitation is that the spectrum can only be recorded with a frequency step of the FSR value. Since the calibration of relative frequency intervals is generally more important in quantitative measurements of gas content, this method is widely used in applications of trace gas detection.

However, the cavity modes may have frequency jitters during the measurement due to mechanical vibration or temperature drift. In order to stabilize the cavity modes, Hodges et al. (2004) locked the cavity length with a He−Ne laser. Two-color HR mirrors were used in such approach, which have not only a high-reflectivity in the CRDS probing wavelength but also a moderate reflectivity (around 95%) at 633 nm. A PID feedback servo was used to control the PZT on an HR mirror, locking a cavity mode at 633 nm with the frequency-stabilized He−Ne laser, thus keeping the cavity length locked during spectral scan. This method eliminates frequency drift of the cavity modes and enables accurate quantitative measurements. The Doppler shift due to the moving mirrors is also avoided. A disadvantage is that customized two-color HR mirrors are needed. In addition, the stability of the cavity length, therefore the frequency accuracy of the cavity mode, is limited by the frequency stability of the He−Ne laser, which is usually at the level of 1 MHz.

In this “dither-laser” mode, it is necessary to optimize the scan range (Chen et al., 2014). If the range is too narrow, it may not be sufficient to match with one cavity mode, and if the range is too broad (exceeding one FSR of the cavity), two adjacent cavity modes may be excited in succession which will induce beating signal similar to that shown in Fig. 8.3(a). There is a need of avoiding the above two situations, improving the efficiency of matching the laser and the cavity, and producing more ring-down events during the measurement. Hodges et al. designed an automated scanning control (Hodges and Ciurylo, 2005) to dynamically control the laser frequency to ensure that the laser is dithering around the preset longitudinal mode of the cavity. In most applications using the near-infrared or visible lasers, the width of a molecular line ranges from a few hundred MHz to a few GHz. Since the FSR of a moderate cavity (i.e., 200 MHz for a 75-cm-long cavity) is smaller than the molecular linewidth, which can be used as the spectral scanning step size, it can actually satisfy the requirement of most quantitative measurements. In this case, the control of spectral scanning can be further simplified (Chen et al., 2014).

The above two methods force the laser to periodically resonate with the optical cavity by quickly changing either the cavity length or the laser frequency. They are relatively simple, but the efficiency is low. Since the laser (or cavity length) is scanning, the time duration for the two to maintain resonance is limited. Before the laser power is accumulated to a sufficient level in the cavity, the resonance condition may be lost. As a result, the amplitude of the transmitted light signal is often very low. This periodic resonance is less efficient and generally the repetition rate of the ring-down events is only tens of times per second. One solution is to lock the probe laser with the optical cavity to keep the resonance. When the locking servo is closed, the transmittance of the

optical cavity can quickly reach a steady-state condition described by Eq. (8.10). In principle, it is possible to maintain the lock by a feedback control of either the length of the optical cavity or the laser frequency. Since the cavity length adjustment generally relies on the PZT which usually has a limited bandwidth, while the feedback bandwidth of the laser could reach a few MHz by quite a few different means, the latter is more commonly used. A widely applied method is to lock the laser frequency with the cavity by the Pound-Drevor-Hall (PDH) method (Drever et al., 1983), provided that the laser has a narrow linewidth and the feedback servo has sufficient bandwidth. Commercial distributed-feedback (DFB) diode lasers are usually more difficult to lock on high-finesse optical cavities due to their broad linewidth (a few MHz). The difficulty has been circumvented by Kassi and his coworkers (Burkart et al., 2014), who developed a feed-forward method to lock the DFB laser with a stable "V"-shape cavity. Usually, external-cavity diode lasers (ECDLs) have narrower linewidths and it can be easier to lock to those cavities.

Fig. 8.7 shows the procedure used by Wang et al. (2017b) to do CRDS measurements using a laser locked with the cavity. An ECDL laser was first locked with the cavity by the PDH method and then chopped off to produce ring-down events. It can be seen that when the laser is turned on and the PDH lock loop is closed, the light field in the cavity is gradually established, and the transmitted light intensity is increased, and then stabilized within 1 millisecond (depending on the finesse of the optical cavity). When the incident light is cut off, the PDH loop is broken, a ring-down signal is generated. In this way, the laser frequency was locked with the ring-down cavity, but the efficiency is reduced due to the need of repeatedly switching on/off the PDH locking loop.

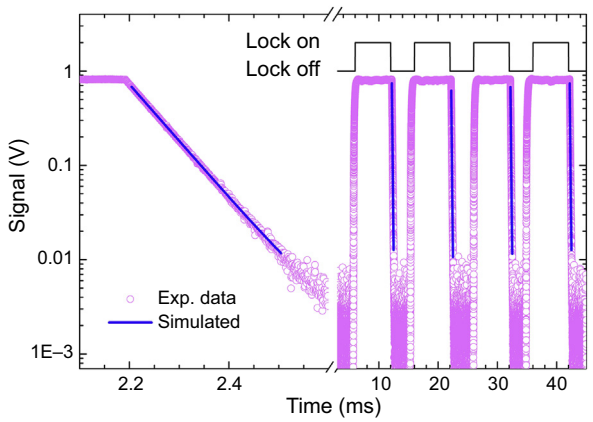

FIGURE 8.7 The CRDS data with the probe laser frequency locked on the cavity. The open circles show the recorded signal and the solid line on the top of the circles is the simulated exponential decay curve. The corresponding locking control sequence is shown above the ring-down data. *Figure reprinted with permission from Wang, J., Sun, Y.R., Tao, L.G., Liu, A.W., Hua, T.P., Meng, F., Hu, S.M., 2017b. Comb-locked cavity ring-down saturation spectroscopy. Rev. Sci. Instrum. 88, 043108. Copyright 2017 AIP.*

8.2.4 Limit of detection

The measurement sensitivity of CRDS measurements is the primary concern in trace detection applications. It is related to many factors in the experiment, such as the design of the optical cavity, signal acquisition, etc., which will be analyzed one by one below.

The sensitivity of a CRDS instrument or the minimum detectable absorption is often described by the noise-equivalent absorption coefficient (NEAC). According to Eqs. (8.1) and (8.2), it could be written as

$$\delta\alpha = \frac{\delta\tau}{\tau}\frac{1-R}{L}. \tag{8.15}$$

A moderate CRDS instrument can measure the decay time τ to a fractional uncertainty $\frac{\delta\tau}{\tau} \sim 10^{-3}$, which is usually limited by the electronic noise of the PD and the resolution of the digitizer. The use of HR mirrors with higher reflectivity and a ring-down cavity with larger length usually leads to better sensitivity. However, a long cavity will reduce the stability, and also limits applications where a miniature instrument is required. Meanwhile, mirrors with higher reflectivity are also more sensitive to contamination, which reduces the robustness of the device. A cavity with a very high finesse may also lead to a decrease in the transmittance of the cavity (Eq. 8.10), which increases the detector noise. In CRDS measurements, it is necessary to use low-loss HR mirrors to get sufficient light power transmitted from the cavity. At present, the reflectivity of commercially available HR mirrors can be in the range of 99.9%–99.999% and the mirror loss can be as low as several parts per million, but the difficulty of coating increases quickly with the reflectivity. One have to balance the sensitivity and convenience of the CRDS instrument. According to Eq. (8.15), a CRDS device with a 50 cm long cavity and HR mirrors of 99.995% will have a typical sensitivity of 10^{-9} cm^{-1} per ring-down event.

8.2.4.1 Fringes

Interference between reflections from surfaces in the optical path causes the light intensity to vary with frequency. When the reflectivity is large, the étalon effect is very obvious, as shown in Fig. 8.2, and even tiny interference due to accidental scattering can induce observable influence in the measurement. The étalon effect can be observed in most spectrometers and its drift during the measurement often limits the performance of the experimental setup (Werle, 2011). Because the CRDS method detects very small changes of the loss in the optical path, it is very sensitive to the étalon effect, which is usually called “fringes” in the spectrum.

Fig. 8.8 shows a typical fringe observed in a piece of ring-down spectrum. There is a clear periodic structure, the period is 0.55 cm^{-1} and the peak-to-peak amplitude is about 2×10^{-9} cm^{-1}. Fig. 8.9 gives another example, which shows the spectrum of a C_2H_2 line at 795 nm, and it seems to have a good signal-to-noise ratio of over 1000. However, after the spectrum was fitted by a Voigt profile, we can see evident multiple periodic structures in the fitting residuals. The fringe structure often drifts slowly with the

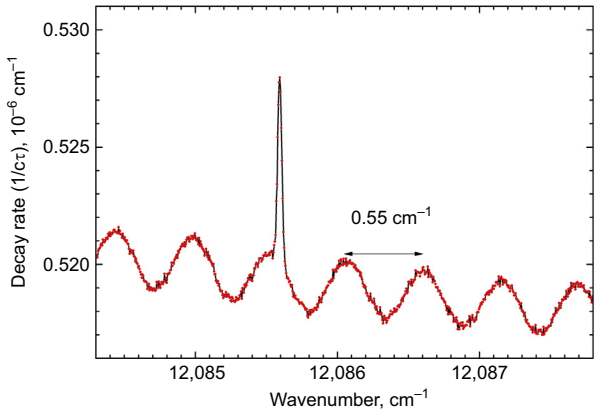

FIGURE 8.8 Fringes observed in a piece of cavity ring-down spectrum. There is a water line at 12,085.6 cm^{-1}. The cyclic pattern with a period of 0.55 cm^{-1} is the so-called "fringe" due to the interference between the two sides of an HR mirror.

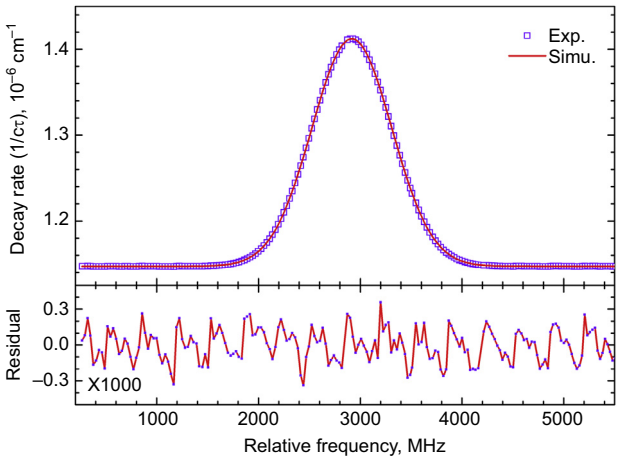

FIGURE 8.9 Example of small fringes observed in a piece of cavity ring-down spectrum around an absorption line of C_2H_2 at 795 nm. The molecular spectral line was fitted by a Voigt profile and the periodic pattern of fringes is visible in the fitting residuals.

environment around the spectrometer, can hardly be removed by averaging, and eventually raises the noise level in the measurement. Some studies have been applied to remove the fringes by taking into account étalons of different periods in the spectral fitting (Cygan et al., 2012; Truong et al., 2015). For example, in the study by Truong et al. (2015), six étalons were applied in the fit of a piece of spectrum in a frequency range of several GHz. However, there is always a concern on the correlation between the parameters of the absorption lines and the fringes, which may induce systematic shifts to the results derived from the fit.

It is preferred to reduce the fringe effect by eliminating the interference between surfaces in the optical path. Characters of the étalon can be found from the fringe spectrum, which could be used to identify the surfaces contributing to the fringe. For example, from the period of the fringes shown in Fig. 8.8, we found that the fringes came from an étalon with an optical distance of about 1 cm. Then we identified that it was due to the interference between two surfaces of one HR mirror. By slightly moving the HR mirror to avoid the normal reflection from the back side of the HR mirror, we successfully reduced the fringe amplitude to below the noise level. Another commonly applied method (Kassi et al., 2005; Gao et al., 2010) is to introduce a fast vibration in the optical path, which actually changes quickly the phase of the fringes and eliminates the fringes in the averaged signal.

8.2.4.2 Repetition rate of ring-down events

Although the signal-to-noise ratio of a single ring-down event is limited, if more ring-down events are generated, it is possible to effectively reduce the statistical noise and increase the sensitivity. In the "dither-mirror" and "dither-laser" modes discussed above, since it takes time for scanning and building the optical field inside the cavity, the repetition rate of the ring-down events can hardly reach 100 per second. As the measurement duration of each ring-down event is only a few hundred microseconds, the effective measurement time is relatively low.

Paldus et al. (1998) divided the laser into two beams with different polarizations, one for keeping the laser locked on the cavity, and the other for measuring the ring-down signal, and they achieved a ring-down repetition rate of 50 kHz. Spence et al. (Spence et al., 2000) further improved the acquisition system and enhanced both the spectral scanning range and the measurement sensitivity. However, they used a relatively low-finesse cavity and the ring-down time was only a few microseconds, which limited the sensitivity of the apparatus. Hodges' group applied the PDH method to lock the probe laser on the cavity, and achieved a repetition rate of a few kHz (Cygan et al., 2011).

We also developed a laser-locked CRDS method in which we locked the laser frequency to a longitudinal mode of the ring-down cavity. Two separated beams were used, one for PDH locking the laser with the ring-down cavity, and the other one for CRDS detection which could be switched on and off periodically. By using the "double-beam" method, we could increase the repetition rate of the ring-down events to over 10 kilohertz which is in principle only limited by the duration of the decay curve (Wang et al., 2017a). Note that the frequencies of the "locking" and "probing" beams are not necessarily identical. In order to avoid interference between the two, on the one hand, polarization of one beam was set perpendicular to the other one; and on the other hand, a combination of AOM and EOM was used to shift the laser frequency on the probing path. The frequency shift was set exactly equal to an integer multiple of the FSR value of the cavity, which keeps the cavity transparent to the "probing" beam as long as the "locking" beam is locked with the cavity. In this way, we also considerably improved the efficiency of coupling the probing laser into the optical cavity. The cavity length can be further

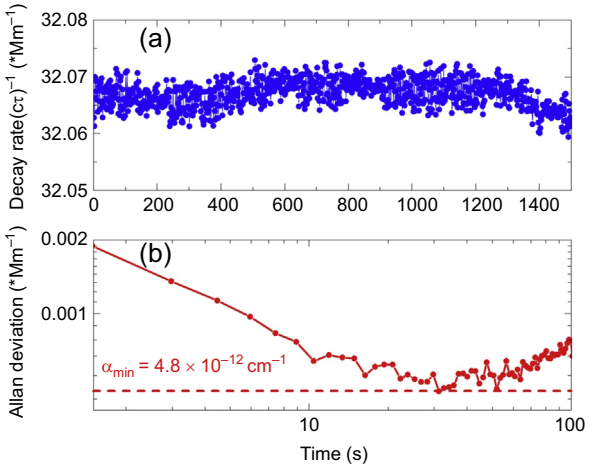

FIGURE 8.10 Sensitivity (noise-equivalent absorption coefficient, NEAC) of a laser-locked CRDS instrument. The optimal NEAC reaches 4.8×10^{-12} cm^{-1} at an averaging time of 30 s. (a) A continuous measurement of the decay rate $\left(\frac{1}{c\tau}\right)$. (b) Allan deviation of the measured decay rate. *Figure reprinted with permission from Kang, P., Wang, J., Liu, G.L., Sun, Y.R., Zhou, Z.Y., Liu, A.W., Hu, S.M., 2018b. Line intensities of the 30011e–00001e band of $^{12}C^{16}O_2$ by laser-locked cavity ring-down spectroscopy. J. Quant. Spectrosc. Radiat. Transf. 207, 1–7. Copyright 2018 Elsevier.*

stabilized by using stable optical references, either a frequency comb or a stabilized narrow-linewidth laser, which eventually stabilizes the probe laser frequency for precision measurements. Fig. 8.10 shows a continuous measurement using such a CRDS instrument based on a cavity of 110 cm long and a pair of HR mirrors of $R = 0.99996$. The sensitivity (NEAC) is 2×10^{-11} cm^{-1} at one second and reaches 4.8×10^{-12} cm^{-1} at an averaging time of 30 s. During the spectral scan, the change of FSR is negligible compared to the width of the cavity mode which is a few kilohertz, and we can perform measurements with sub-kHz frequency accuracy for a continuous scan of tens of GHz.

8.2.4.3 *Long-term averaging*

We can also see that from Fig. 8.10, the long-term drift of the baseline, rising from miscellaneous sources, such as slowly changing fringes, limits the improvement of the sensitivity by averaging more ring-down events at a fixed frequency. The difficulty can be overcome by spectral averaging. If each spectral scan could be accomplished within a short period, the baseline could be considered stable during the scan. Therefore, the profile of the absorption line remains in each scan. The content of target gas, which is derived from the fit of the averaged spectrum, could be immune to the baseline drift. Therefore, by increasing the averaging number N, the LOD could be improved better than the sensitivity at a fixed frequency that shown as the minimum in the Allan deviation plot in Fig. 8.10.

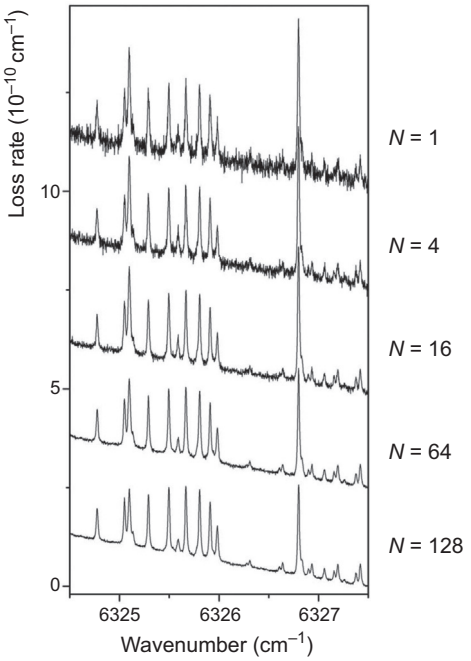

FIGURE 8.11 Averaged spectra of the O_2 molecule in the region of the ^{Q}Q branch of the $a^1\Delta_g(0) - X^3\sum_g^-(1)$ hot band. *N* presents the number of averaged scans. The sample oxygen gas pressure was regulated at 100 Torr. Each scan took about 13 min. *Figure reprinted with permission from Kassi, S., Campargue, A., 2012. Cavity ring down spectroscopy with 5×10^{-13} cm^{-1} sensitivity. J. Chem. Phys. 137, 234201. Copyright 2012 AIP.*

Kassi and Campargue demonstrated days-long averaging of recorded ring-down spectra to improve the LOD. They recorded the ^{Q}Q branch of the $a^1\Delta_g(0) - X^3\sum_g^-(1)$ hot band of O_2 at 1.58 μm. The spectrum covering 9 cm^{-1} was acquired from 180 scans accomplished in 40 h. Fig. 8.11 shows the averaged spectra versus the averaging number *N*. The increase of *N* considerably reduces the noise level in the averaged spectrum and decreases the LOD value down to 1.2×10^{-12} cm^{-1}. They applied the same strategy to record the extremely weak electric quadrupole transition in the (3−0) band of N_2 near 1.44 μm. The spectra of a single scan and an average of over 6000 scans are shown in Fig. 8.12. The N_2 line and a line of $H_2^{18}O$ are below the noise level of single scan but clearly visible from the averaged spectrum. Water vapor presented as a minor (<1 ppm) contaminant in the nitrogen gas sample. In total, 6220 spectra, each covering a range of 0.5 cm^{-1}, were accumulated in 4.6 days. As demonstrated in that study, the LOD value decreased as a function of $\sqrt{N}$ and reached the level of 10^{-13} cm^{-1}. They did not see any limit during their days-long measurements.

8.3 Application of CRDS for trace detection of molecules

The CRDS technology has been widely applied for the detection of trace gases, because of its high detection sensitivity and fast response. The content of the target molecule can be derived from the CRDS measurement:

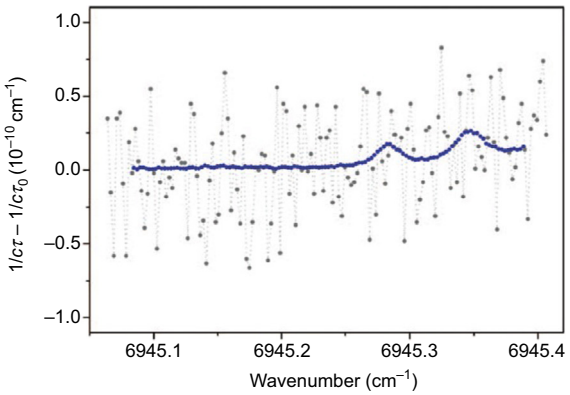

FIGURE 8.12 Spectra of a single scan (gray dots) and an average of 6220 scans (blue (dark gray in print version) dots) recorded at 1.44 μm. The sample gas was pure nitrogen (80 Torr). Two lines were observed in the averaged spectrum: the left one is the S4 electric quadrupole transition in the (3—0) band of N_2, and the right one is a water line which presents as a minor (0.5 ppmv) contaminant in the sample. *Figure reprinted with permission from Kassi, S., Campargue, A., 2012. Cavity ring down spectroscopy with 5×10^{-13} cm^{-1} sensitivity. J. Chem. Phys. 137, 234201. Copyright 2012 AIP.*

$$\alpha(\nu) = kn\phi(\nu) \tag{8.16}$$

where k is the strength of the absorption line, and $\phi(\nu)$ is the function of the line profile, which is usually a convolution of the Doppler broadening and pressure broadening. Since the absorption coefficient α is directly determined in CRDS (Eq. 8.1), if the line strength is known, the molecular number density, n, can be directly determined without calibration with standard samples. Therefore, the method is particularly useful when a standard sample is not available. Many research groups have built different devices to measure the content of various trace substances. There have already been some successfully commercialized instruments based on CRDS for detecting gases such as water, CO_2, CH_4, and their stable isotopes. Here we just give a brief introduction to some scientific studies on detecting gaseous molecules and radicals. It is impossible to completely cover all relevant work, so we just give some representative examples here, and more related studies can be found in the cited references.

8.3.1 Greenhouse gases

Greenhouse gases are the most common objects in gas detection applications. They mainly include water (H_2O), carbon dioxide (CO_2), methane (CH_4), nitrous oxide (N_2O), sulfur hexafluoride (SF_6), hydrofluorocarbon (HFCs), and perfluorocarbon (PFCs).

8.3.1.1 H_2O

The contribution of water vapor to the atmospheric greenhouse effect is the most pronounced. However, since water vapor participates in the water cycle on the earth, the water vapor content in the atmosphere is not related to human activities. The discussion

of "enhancing the greenhouse effect" does not take into account the effects of water vapor. Since water vapor is ubiquitous, quantitative monitoring of trace water vapor (humidity) is also important for many industrial production activities. Various hygrometers based on different principles have a long history of development. Water molecules have a large number of absorption lines with different transition strengths in the infrared which can be used for the spectroscopic detection. Lehman et al. from the National Institute of Standards and Technology (NIST) demonstrated the detection of the water vapor content of sub-ppm level in phosphine (PH_3) through the CRDS measurement of the water line at 10,667.76 cm^{-1} (Lehman et al., 2004). Absorption lines of the water molecule near 1.36 and 1.39 microns have intensities at the level of 10^{-20} cm/molecule, and mature DFB semiconductor lasers are also available in these wavelengths. These lines are often used to measure trace amounts of water vapor by CRDS. Hodges and Lisak (2006) from NIST presented a detection limit of 0.7 ppbv (10 min averaging time) using the water line at 7181.156 cm^{-1}. Fiadzomor et al. (2008) from the University of Bristol built a cw-CRDS device capable of measuring the water vapor content of a few tens ppbv in N_2, CF_4, SiH_4, and PH_3. The same water line was also used by Abe and Yamada from the National Institute of Metrology of Japan (NMIJ) to detect trace water vapor with a detection limit of 1 ppbv (Abe and Yamada, 2011) and subsequently improved to 12 pptv (Hashiguchi et al., 2016). We have also demonstrated (Chen et al., 2015) a detection limit of 8 pptv using a cw-CRDS device operated near 1.363 μm.

8.3.1.2 CO_2

Carbon dioxide (CO_2) is the most important greenhouse gas that affects the Earth's radiation balance. It is also a reference gas molecule that measures the warming potential of other greenhouse gases and its emission limits are included in the Kyoto Protocol. The sources of carbon dioxide in the atmosphere are divided into natural sources and anthropogenic sources. Natural sources mainly include sea-air exchange, animal and plant respiration and corruption, biomass burning, etc. Anthropogenic sources mainly include fossil fuel combustion and land use change. The global average concentration in the year 2008 increased by 38% compared with 1750, far exceeding the natural carbon dioxide concentration in last 650,000 years according to the ice core record. Absorption lines of CO_2 in the 1.5 to 1.6 μm region, having a strength at the level of 10^{-23} cm/molecule, are often used to detect carbon dioxide including its isotopologues (Awtry and Miller, 2002; Crosson et al., 2002; Crunaire et al., 2006; Wang et al., 2008; Chen et al., 2014).

8.3.1.3 CH_4

Methane (CH_4) is the second important greenhouse gas in the atmosphere. The potential for warming per unit CH_4 molecule is about 20 times that of carbon dioxide. It is also included in the Kyoto Protocol's limit list. The main source of methane in the atmosphere is the fermentation process of anaerobic bacteria, and the leakage of crude oil and natural gas also releases a large amount of methane. Most of the methane currently

emitted into the atmosphere is oxidized by hydroxyl radicals, but the remaining methane has also caused an increase of concentration in the atmosphere. The global average concentration of methane in 2008 has reached 1797 ppbv, an increase of 157% compared to the year 1750.

Instruments of cw-CRDS were developed to detect methane using diode lasers at 1653 nm (Fawcett et al., 2002; Chen et al., 2013; Wang et al., 2019) and at 1742 nm (McHale et al., 2016) and quantum cascade lasers (QCLs) in the midinfrared region of 7.8 μm (Hamilton and Orr-Ewing, 2011; Maity et al., 2017). A detection limit of CH_4 as low as 10 pptv has been demonstrated (Chen et al., 2013).

8.3.1.4 N_2O

Nitrous oxide (N_2O), commonly known as laughing gas, is the highest nitrogen-containing compound in the lower atmosphere. Its potential for warming per unit molecule is about 300 times that of carbon dioxide. It is also one of the greenhouse gases limited by the Kyoto Protocol. The natural source of nitrous oxide is mainly the release of marine and tropical forests. Anthropogenic sources are mainly agricultural production processes, industrial production, and livestock emissions, accounting for more than 1/3 of the total emissions. Nitrous oxide can only be eliminated by slow photolysis in the stratosphere, and therefore has a long lifetime of about 120 year in the atmosphere. The concentration of nitrous oxide has been maintained at around 270 ppbv for more than 1000 years before the industrial revolution but increased at a rate of 0.2%−0.3% per year after that. By 2008, the global average concentration of nitrous oxide has reached 321.8 ppbv.

Because the N_2O concentration in the atmosphere is relatively low and its absorption bands in the near-infrared are relatively weak, optical detection of N_2O mainly uses its absorption lines in the midinfrared, including those lines at 4.5 μm (Fleisher et al., 2017), 5.2 μm (Banik et al., 2018), and 7.7 μm (Wojtas et al., 2013). QCLs were applied in these studies, and the detection limit of N_2O can reach 2 ppbv.

8.3.2 Reactive gases

In addition to the substances mentioned above, there are other gases in the atmosphere that have an impact on weather, climate, environment, and human health. Ground and tropospheric ozone, sulfur dioxide (SO_2), nitrogen oxides, carbon monoxide (CO), ammonia (NH_3), volatile organic compounds (VOCs), peroxyacyl nitrates (PANs), hydrogen peroxide (H_2O_2), and various reducing sulfides and free radicals are all reactive gases which usually have a lifetime less than 1 year in the atmosphere. Carbon monoxide, sulfur dioxide, ammonia, and other substances are known harmful to human body, and they also produce some secondary pollutants through photochemical reactions, or convert them into acid rain, destroying ecosystems and building materials. Therefore, the detection of contents of these molecules has also attracted increasing interests.

8.3.2.1 NO_y

Total reactive nitrogen (NO_y) includes NO_x (NO, NO_2) and all its oxidation products, such as NO_3, N_2O_5, HONO, HNO_3, PNs (peroxynitrate, RO_2NO_2), ANs (alkyl nitrates, $RONO_2$), PANs (peroxyacetyl nitrates, $RCOOONO_2$), etc., wherein the NO_x-removing portion may also be collectively referred to as NO_z. These substances have high reactivity and participate in various reactions in atmospheric chemical processes. The formation of common pollution phenomena such as acid rain, photochemical smog, secondary aerosol, and other pollutants are related to reactive nitrogen. The main sources of NO_x in the atmosphere include fossil fuel combustion (industrial production, automobile exhaust, smelters, power plants, etc.), biomass burning, lightning processes, stratospheric photochemical reactions, in which emissions from human activities are the main source of nitrogen oxides. The peroxynitrate, alkyl nitrate, nitric acid, and the like in the atmosphere are usually intermediates or final products derived from the reaction of NO_x with VOCs. Most of these substances are harmful to living organisms. For the human body, they will damage the mucous membranes, thus harming important organs such as the respiratory tract and even destroying the central nervous system. Long-term inhalation will cause permanent damage to the human body. Among them, the harm of nitrogen dioxide is particularly obvious.

Optical detection of NO_2 often uses its strong electronic absorption bands near 410 nm (Wada and Orr-Ewing, 2005; Wojtas and Bielecki, 2008; Stacewicz et al., 2012; Wojtas et al., 2013; Chen et al., 2017), 450 nm (Ling et al., 2013), 532 nm (Osthoff et al., 2006), and 625 nm (Ventrillard-Courtillot et al., 2010). By converting some NO_z species to NO_2, some of the methods and devices for detecting NO_2 given in the references above can be used to detect NO_z, such as RONO (Thieser et al., 2016; Chen et al., 2017) and HONO (Min et al., 2016). Fig. 8.13 shows an example of ambient detecting NO_2 and RONO. The 405 nm absorption band of NO_2 was applied in the CRDS measurement. RONO was detected simultaneously with a separated channel by converting RONO to NO_2 through thermal dissociation. Since the commonly used NO_x analyzer based on chemiluminescence detection of NO converts both RONO and NO_2 to NO, it cannot distinguish RONO from NO_2 in ambient samples.

NO_3 has a very high reactivity and a low concentration of a few pptv or less in ambient air. Its strong absorption band near 662 nm is often used for optical detection (Dubá et al., 2006; Odame-Ankrah and Osthoff, 2011; Flemmer and Ham, 2012). Wagner et al. (2011) developed a portable CRDS system which detects NO_3 with a sensitivity of 3 pptv (2σ, 1s). N_2O_5 can also be detected after converting it to NO_3 through pyrolysis.

Vibronic transitions of these nitrogen oxides molecules are usually broad and overlap with the bands of some interfering molecules, which limit the accuracy of the measurement. Incoherent broadband cavity-enhanced absorption spectroscopy (IBBCEAS) has also been used to detect NO_3 (Venables et al., 2006; Langridge et al., 2008; Kennedy et al., 2011), which takes the advantage of resolving the absorption of NO_3 from the overlapping lines of water and NO_2 at 662 nm. Kennedy et al. from the Cambridge

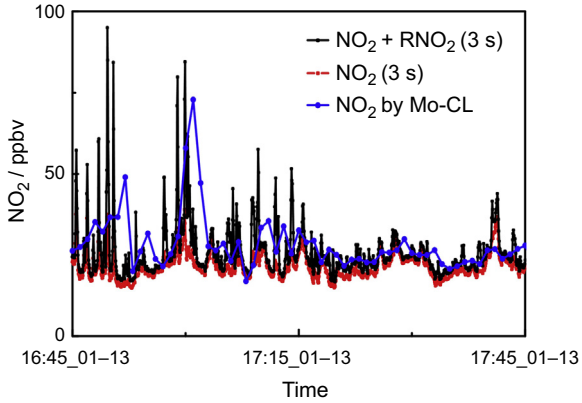

FIGURE 8.13 Ambient concentration of NO_2 detected by CRDS, compared with that by a commercial NO analyzer. A two-channel CRDS instrument was used, one channel for detecting NO_2 and the other channel for RONO by converting RONO to NO_2 through thermal dissociation. The absorption band of NO_2 at 405 nm was used for CRDS measurement. The commercial NO_x analyzer (Thermo Fisher Scientific, 42i-TL), equipped with molybdenum converter, is based on the chemiluminescence (Mo-CL) detection of NO. *Figure reprinted with permission from Chen, J., Wu, H., Liu, A.W., Hu, S.M., Zhang, J., 2017. Field measurement of NO_2 and RNO_2 by two-channel thermal dissociation cavity ring down spectrometer. Chin. J. Chem. Phys. 30, 493–498. Copyright 2017 Chinese Physics Society.*

University used IBBCEAS to detect NO_2, NO_3, and N_2O_5, and obtained a detection limit of 0.17 pptv (830 s averaging time) for NO_3 (Kennedy et al., 2011).

It is also worth noting that relatively narrow infrared transitions are also possible choices for measuring nitrogen oxides. Banik et al. developed a CRDS instrument using a QCL laser at 5.2 μm for optical detection of NO and N_2O (Banik et al., 2018). Jain et al. from the University of Lille built a cw-CRDS device to measure the concentration of nitrous acid (Jain et al., 2011) using its ro-vibrational lines around 6643 cm^{-1}.

8.3.2.2 O_3

Ozone is mainly distributed in the stratosphere, with the highest concentration at the height of 20–25 km, which is called the "ozone layer." The stratospheric ozone can absorb almost all of the solar ultraviolet radiation with a wavelength in the range of 200–300 nm, which has a protective effect on the biosphere. Ozone has a strong oxidizing effect, and ozone in the troposphere is harmful to living organisms and is one of the main causes of photochemical smog. Nitrogen oxides and hydrocarbons, natural or anthropogenic, can generate ozone under the action of sunlight and are the main source of tropospheric ozone. The CRDS measurement of ozone is mostly indirect by converting ozone into other molecules in a known ratio. For example, Washenfelder et al. converted ozone to nitrogen dioxide with excess nitric oxide, and the absorption of nitrogen dioxide at 404 nm was measured to determine the concentration of ozone. They reported a detection limit of ozone of 28 pptv (1s, 2σ) (Washenfelder et al., 2011).

8.3.2.3 VOC

Organic compounds which are present in gaseous form at normal temperature are referred to as VOCs. VOCs are generally classified into nonmethane hydrocarbons (NMHCs), oxygen-containing organic compounds, halogenated hydrocarbons, nitrogen-containing organic compounds, and sulfur-containing organic compounds.

Acetylene (C_2H_2) is a trace VOC in the atmosphere that is almost entirely from anthropogenic sources. Because it is relatively stable under photocatalytic oxidation, acetylene has a longer lifetime than other atmospheric hydrocarbon compounds. Therefore, acetylene is an important tracer for polluted air masses. The concentration of acetylene in the troposphere is usually about 0.8−2.5 ppbv in rural areas and reaches 150 ppbv in urban areas.

C_2H_2 lines near 1.53 μm have strengths at the level of $k \sim 10^{-21}$ cm/molecule, and they were frequently used to detect trace acetylene in the air. Parkes et al. from the University of Bristol reported a C_2H_2 detection limit of 6 ppbv using a CRDS device (Parkes et al., 2003). They also demonstrated the detection of C_2H_4, 1-butene, 2-methyl propylene, and 1,3-butadiene using transitions of these molecules near 1625 nm.

The detection sensitivities for ethylene and acetylene were further improved by preconcentration of air samples with an adsorbent trap prior to CRDS measurements (Parkes et al., 2004). Pradhan et al. (2008) demonstrated a limit of 35 pptv detecting acetylene with a cw-CRDS device operated near 1535 nm. Halonen's group at the University of Helsinki also demonstrated CRDS detection of acetylene with sub-ppbv sensitivity (Schmidt et al., 2010), and subsequently developed a CRDS device for respiratory monitoring of hydrogen cyanide (HCN), ammonia (NH_3), and acetylene (C_2H_2) (Vaittinen et al., 2013).

Acetone (CH_3COCH_3) is the simplest saturated ketone. It is a metabolic substance in the human body. The concentration of acetone in exhaled breath can be used as an indicator of certain diseases. In the atmosphere, most of the acetone comes from natural processes, such as plant decay and forest fires, also comes from human activities such as industrial emissions. Wang and Surampudi (2008) from the University of Mississippi developed a portable respiratory monitor of acetone based on the CRDS measurement at 266 nm, and they obtained a detection limit of 0.13 ppmv. Bicer et al. (2018) built a CRDS device in the near-infrared region and achieved a detection limit of 2.1 ppbv for acetone.

Methyl iodide (CH_3I) is a marine source toxic halogenated hydrocarbon and also used in many industrial and agricultural applications. Its quantitative analysis mainly depends on gas chromatography and mass spectrometry or electron capture detector phase. Sadiek et al. (2017) from the University of Keele built a midinfrared CRDS device using the transition at 3090.4289 cm^{-1} to detect methyl iodide, and obtained a noise-equivalent detection limit of 15 ppbv, which is suitable for leak detection and reaction process studies.

Human skin cells also release VOCs, some of which can be used as biomarkers for screening specific diseases, such as dimethyl disulfide (DMDS), as a biomarker for

melanoma skin cancer. Wang et al. (2016) set up a CRDS device working at 266 nm to detect dimethyl disulfide in the ppmv to pptv range.

8.3.2.4 Other reactive molecules

Besides the atmospheric molecules mentioned above, there are some trace reactive molecules and radicals that also have important impact on climate, pollution, and health. They include CO, SO_2, H_2O_2, hydroxyl radical (HO•), alkoxy radicals (RO•), peroxy radicals (HO_2• and RO_2•), etc. Some representative studies using CRDS to detect these molecules and radicals are given in Table 8.1.

8.4 Summary

CRDS is one of the cavity-enhanced absorption spectroscopy methods using a high-finesse optical cavity to increase the effective absorption path length. In CRDS, the decay curve is measured instead of the transmittance of the cavity, which also reduces the influence due to laser power noise. The detectable minimum absorption coefficient can easily reach the level less than 10^{-7} cm^{-1}. By using cw lasers for single mode excitation, the sensitivity of cw-CRDS devices can be further improved, and the best reported sensitivity reaches 10^{-13} cm^{-1}. As an absorption spectroscopy method, CRDS directly measures the absorption coefficient of the sample gas, which is a great advantage for quantitative trace detection. Since the sample cell used in CRDS has a simple structure and does not require a complicated multipass optical scheme, it is possible to miniaturize the sample cell. For some applications where the sample volume is limited, the CRDS method is very competitive.

Table 8.1 Atmospheric molecules and radicals detected by CRDS.

	Wavelength (nm)	Limit of detection	References
CO	4600	3 ppbv	Nwaboh et al. (2012)
SO_2	308	3.5 ppbv	Medina et al. (2011)
HCN	1036	2.5×10^{13} cm^{-3}	Lamoureux et al. (2013)
NH_3	6200	0.74 ppbv	Maithani et al. (2018)
$C_6H_5CH_2$	450	1×10^{11} cm^{-3}	Tonokura and Koshi (2003)
OIO	570	4 pptv	Bitter et al. (2005)
C_6H_5	504.8		Park et al. (2006)
SH	323		Buzaianu et al. (2008)
CS	259		Buzaianu et al. (2008)
OH	308	6.6×10^{10} cm^{-3}	Srivastava and Wang (2011)
HO_2/NO_2	408.9	3 pptv	Horstjann et al. (2014)
HO_2	1506.4	7.4×10^{8} cm^{-3}	Gianella et al. (2016, 2018)
BrO	317.5	6×10^{11} cm^{-3}	Wheeler et al. (1998)
IO	435	10 pptv	Wada et al. (2007)

Applications of the CRDS in trace detection have covered almost all the regions from infrared to ultraviolet, and various laser sources have been used. If the coupling of the laser to the optical cavity is well controlled, a cw milliwatt laser is sufficient for high-sensitivity CRDS detection. Near-infrared semiconductor lasers, particularly the DFB diode lasers, having the advantages of low power consumption, convenient tuning, and low cost, are ideal for CRDS applications. Using QCLs or tunable optical parametric oscillators, the spectral range can be easily extended to the midinfrared region where molecules have stronger absorption lines. There is an increasing interest to develop CRDS in the midinfrared, although the laser sources and detectors are not yet as convenient as those used in the near-infrared. In the ultraviolet region, it is expected to achieve higher detection sensitivity because extremely strong electronic transitions can be used for detection. With the development of ultraviolet lasers, including those upconversion sources, combined with evolving coating technology in producing HR ultraviolet mirrors, we can expect more exciting applications in the near future.

References

Abe, H., Yamada, K.M., 2011. Performance evaluation of a trace-moisture analyzer based on cavity ring-down spectroscopy: direct comparison with the NMIJ trace-moisture standard. Sens. Actuator A 165, 230–238.

Anderson, D.Z., Frisch, J.C., Masser, C.S., 1984. Mirror reflectometer based on optical cavity decay time. Appl. Opt. 23, 1238–1245.

Awtry, A.R., Miller, J.H., 2002. Development of a cw-laser-based cavity-ringdown sensor aboard a spacecraft for trace air constituents. Appl. Phys. B 75, 255–260.

Banik, G.D., Maity, A., Som, S., Pal, M., Pradhan, M., 2018. An external-cavity quantum cascade laser operating near 5.2 μm combined with cavity ring-down spectroscopy for multi-component chemical sensing. Laser Phys. 28, 045701.

Berden, G., Engeln, R., 2009. Cavity Ring-Down Spectroscopy: Techniques and Applications. Wiley.

Berden, G., Peeters, R., Meijer, G., 2000. Cavity ring-down spectroscopy: experimental schemes and applications. Int. Rev. Phys. Chem. 19, 565–607.

Bicer, A., Bounds, J., Zhu, F., Kolomenskii, A.A., Kaya, N., Aluauee, E., Amani, M., Schuessler, H.A., 2018. Sensitive spectroscopic analysis of biomarkers in exhaled breath. Int. J. Thermophys. 39, 69.

Bitter, M., Ball, S.M., Povey, I.M., Jones, R.L., 2005. A broadband cavity ringdown spectrometer for in-situ measurements of atmospheric trace gases. Atmos. Chem. Phys. Discuss. 5, 2547–2560.

Born, M., Wolf, E., 1999. Principles of Optics, seventh ed. Cambridge University Press. ISBN 0-521-642221.

Brown, S.S., 2003. Absorption spectroscopy in high-finesse cavities for atmospheric studies. Chem. Rev. 103, 5219–5238.

Burkart, J., Romanini, D., Kassi, S., 2014. Optical feedback frequency stabilized cavity ring-down spectroscopy. Opt. Lett. 39, 4695–4698.

Buzaianu, M.D., Makarov, V.I., Morell, G., Weiner, B.R., 2008. Detection of SH and CS radicals by cavity ringdown spectroscopy in a hot filament chemical vapor deposition environment. Chem. Phys. Lett. 455, 26–31.

Chen, B., Sun, Y.R., Zhou, Z.Y., Chen, J., Liu, A.W., Hu, S.M., 2014. Ultrasensitive, self-calibrated cavity ring-down spectrometer for quantitative trace gas analysis. Appl. Opt. 53, 7716–7723.

Chen, B., Wang, J., Sun, Y.R., Kang, P., Liu, A.W., Li, J.Y., He, X.L., Hu, S.M., 2015. Broad-range detection of water vapor using cavity ring-down spectrometer. Chin. J. Chem. Phys. 28, 440–444.

Chen, J., Wu, H., Liu, A.W., Hu, S.M., Zhang, J., 2017. Field measurement of NO_2 and RNO_2 by two-channel thermal dissociation cavity ring down spectrometer. Chin. J. Chem. Phys. 30, 493–498.

Chen, Y., Lehmann, K.K., Kessler, J., Lollar, B.S., Lacrampe Couloume, G., Onstott, T.C., 2013. Measurement of the $^{13}C/^{12}C$ of atmospheric CH_4 using near-infrared (NIR) cavity ring-down spectroscopy. Anal. Chem. 85, 11250–11257.

Crosson, E.R., Ricci, K.N., Richman, B.A., Chilese, F.C., Owano, T.G., Provencal, R.A., Todd, M.W., Glasser, J., Kachanov, A.A., Paldus, B.A., Spence, T.G., Zare, R.N., 2002. Stable isotope ratios using cavity ring-down spectroscopy: determination of $^{13}C/^{12}C$ for carbon dioxide in human breath. Anal. Chem. 74, 2003–2007.

Crunaire, S., Tarmoul, J., Fittschen, C., Tomas, A., Lemoine, B., Coddeville, P., 2006. Use of cw-CRDS for studying the atmospheric oxidation of acetic acid in a simulation chamber. Appl. Phys. B 85, 467–476.

Cygan, A., Lisak, D., Masowski, P., Bielska, K., Wjtewicz, S., Domysawska, J., Trawiski, R.S., Ciuryo, R., Abe, H., Hodges, J.T., 2011. Pound-Drever-Hall-locked, frequency-stabilized cavity ring-down spectrometer. Rev. Sci. Instrum. 82, 063107.

Cygan, A., Lisak, D., Wójtewicz, S., Domysławska, J., Hodges, J.T., Trawiński, R.S., Ciuryło, R., 2012. High-signal-to-noise-ratio laser technique for accurate measurements of spectral line parameters. Phys. Rev. A 85, 1–11.

Cygan, A., Wcisło, P., Wójtewicz, S., Masłowski, P., Hodges, J.T., Ciuryło, R., Lisak, D., 2015. One-dimensional frequency-based spectroscopy. Opt. Expr. 23, 14472.

Drever, R.W.P., Hall, J.L., Kowalski, F.V., Hough, J., Ford, G.M., Munley, A.J., Ward, H., 1983. Laser phase and frequency stabilization using an optical-resonator. Appl. Phys. B 31, 97–105.

Dubá, W.P., Brown, S.S., Osthoff, H.D., Nunley, M.R., Ciciora, S.J., Paris, M.W., McLaughlin, R.J., Ravishankara, A.R., 2006. Aircraft instrument for simultaneous, in situ measurement of NO_3 and N_2O_5 via pulsed cavity ring-down spectroscopy. Rev. Sci. Instrum. 77, 034101.

Fawcett, B.L., Parkes, A.M., Shallcross, D.E., Orr-Ewing, A.J., 2002. Trace detection of methane using continuous wave cavity ring-down spectroscopy at 1.65 μm. Phys. Chem. Chem. Phys. 4, 5960–5965.

Fiadzomor, P.A., Baker, D.M., Keen, A.M., Grant, R.B., Orr-Ewing, A.J., 2008. Pressure broadening of H_2O absorption lines in the 1.3 μm region measured by continuous wave-cavity ring-down spectroscopy: application in the trace detection of water vapor in N_2, SiH_4, CF_4, and PH_3. Appl. Spectrosc. 62, 1354–1362.

Fleisher, A.J., Long, D.A., Liu, Q., Gameson, L., Hodges, J.T., 2017. Optical Measurement of Radiocarbon below Unity Fraction Modern by Linear Absorption Spectroscopy. In: J. Phys. Chem. Lett, 8, pp. 4550–4556.

Flemmer, M.M., Ham, J.E., 2012. Cavity ring-down spectroscopy with an automated control feedback system for investigating nitrate radical surface chemistry reactions. Rev. Sci. Instrum. 83, 085103.

Gao, B., Jiang, W., Liu, A.W., Lu, Y., Cheng, C.F., Cheng, G.S., Hu, S.M., 2010. Ultra sensitive near-infrared cavity ring down spectrometer for precise line profile measurement. Rev. Sci. Instrum. 81, 043105.

Gianella, M., Reuter, S., Aguila, A.L., Ritchie, G.A., Helden, J.P.H., 2016. Detection of HO_2 in an atmospheric pressure plasma jet using optical feedback cavity-enhanced absorption spectroscopy. New J. Phys. 18, 113027.

Gianella, M., Reuter, S., Press, S.A., Schmidt-Bleker, A., Helden, J.H., Ritchie, G.A., 2018. HO_2 reaction kinetics in an atmospheric pressure plasma jet determined by cavity ring-down spectroscopy. Plasma Sourc. Sci. Techno. 27, 095013.

Hamilton, D.J., Orr-Ewing, A.J., 2011. A quantum cascade laser-based optical feedback cavity-enhanced absorption spectrometer for the simultaneous measurement of CH_4 and N_2O in air. Appl. Phys. B 102, 879–890.

Hashiguchi, K., Lisak, D., Cygan, A., Ciuryło, R., Abe, H., 2016. Wavelength-meter controlled cavity ring-down spectroscopy: high-sensitivity detection of trace moisture in N_2 at sub-ppb levels. Sens. Actuator A 241, 152–160.

Henderson, B., Khodabakhsh, A., Metsala, M., Ventrillard, I., Schmidt, F.M., Romanini, D., Ritchie, G.A.D., Hekkert, S.t.L., Briot, R., Risby, T., Marczin, N., Harren, F.J.M., Cristescu, S.M., 2018. Laser spectroscopy for breath analysis: towards clinical implementation. Appl. Phys. B 124, 161.

Hodges, J.T., Ciurylo, R., 2005. Automated high-resolution frequency-stabilized cavity ring-down absorption spectrometer. Rev. Sci. Instrum. 76, 1–7.

Hodges, J.T., Layer, H.P., Miller, W.W., Scace, G.E., 2004. Frequency-stabilized single-mode cavity ring-down apparatus for high-resolution absorption spectroscopy. Rev. Sci. Instrum. 75, 849–863.

Hodges, J.T., Lisak, D., 2006. Frequency-stabilized cavity ring-down spectrometer for high-sensitivity measurements of water vapor concentration. Appl. Phys. B 85, 375–382.

Hodges, J.T., Looney, J.P., VanZee, R.D., 1996. Response of a ring-down cavity to an arbitrary excitation. J. Chem. Phys. 105, 10278–10288.

Horstjann, M., Hernández, M.D., Nenakhov, V., Chrobry, A., Burrows, J.P., 2014. Peroxy radical detection for airborne atmospheric measurements using absorption spectroscopy of NO_2. Atmos. Meas. Tech. 7, 1245–1257.

Huang, H.F., Lehmann, K.K., 2007. Noise in cavity ring-down spectroscopy caused by transverse mode coupling. Opt. Expr. 15, 8745–8759.

Jain, C., Morajkar, P., Schoemaecker, C., Viskolcz, B., Fittschen, C., 2011. Measurement of absolute absorption cross sections for nitrous acid (HONO) in the near-infrared region by the continuous wave cavity ring-down spectroscopy (cw-CRDS) technique coupled to laser photolysis. J. Phys. Chem. A 115, 10720–10728.

Kang, P., Sun, Y.R., Wang, J., Liu, A.W., Hu, S.M., 2018a. Measurement of molecular absorption spectrum with a laser locked on a high-finesse cavity. Acta Phys. Sinica 67, 104206.

Kang, P., Wang, J., Liu, G.L., Sun, Y.R., Zhou, Z.Y., Liu, A.W., Hu, S.M., 2018b. Line intensities of the 30011e–00001e band of $^{12}C^{16}O_2$ by laser-locked cavity ring-down spectroscopy. J. Quant. Spectrosc. Radiat. Transf. 207, 1–7.

Kassi, S., Campargue, A., 2012. Cavity ring down spectroscopy with 5×10^{-13} cm^{-1} sensitivity. J. Chem. Phys. 137, 234201.

Kassi, S., Romanini, D., Campargue, A., Bussery-Honvault, B., 2005. Very high sensitivity CW-cavity ring down spectroscopy: application to the $a^1\Delta(0) - X^3\Sigma^-_g$ (1) O_2 band near 1.58 μm. Chem. Phys. Lett. 409, 281–287.

Kastler, A., 1974. Transmission of light pulse through a Fabry-Perot interferometer. Nouv. Rev. Optique 5, 133–139.

Kennedy, O.J., Ouyang, B., Langridge, J.M., Daniels, M.J., Bauguitte, S., Freshwater, R., McLeod, M.W., Ironmonger, C., Sendall, J., Norris, O., Nightingale, R., Ball, S.M., Jones, R.L., 2011. An aircraft based three channel broadband cavity enhanced absorption spectrometer for simultaneous measurements of NO_3, N_2O_5 and NO_2. Atmos. Meas. Tech. 4, 1759–1776.

Lamoureux, N., El Merhubi, H., Mercier, X., Pauwels, J.F., Desgroux, P., 2013. HCN quantitative measurement in a laminar low pressure flame at 1036 nm using pulsed CRDS technique. Proc. Combust. Inst. 34, 3557–3564.

Langridge, J.M., Ball, S.M., Shillings, A.J., Jones, R.L., 2008. A broadband absorption spectrometer using light emitting diodes for ultrasensitive, in situ trace gas detection. Rev. Sci. Instrum. 79, 123110.

Lee, J.Y., Hahn, J.W., 2004. Theoretical investigation on the intracavity Doppler effect in continuous wave swept-cavity ringdown spectroscopy. Appl. Phys. B 79, 371–378.

van Leeuwen, N.J., Diettrich, J.C., Wilson, A.C., 2003. Periodically locked continuous-wave cavity ring-down spectroscopy. Appl. Opt. 42, 3670–3677.

Lehman, S.Y., Bertness, K.A., Hodges, J.T., 2004. Optimal spectral region for real-time monitoring of sub-ppm levels of water in phosphine by cavity ring-down spectroscopy. J. Cryst. Growth 261, 225–230.

Lehmann, K.K., Romanini, D., 1996. The superposition principle and cavity ring-down spectroscopy. J. Chem. Phys. 105, 10263–10277.

Ling, L., Xie, P., Qin, M., Hu, R., Fang, W., Zheng, N., Si, F., 2013. Open-path incoherent broadband cavity enhanced absorption spectroscopy for measurements of atmospheric NO_2. Acta Opt. Sinica 33, 0130002.

Ma, L.S., Ye, J., Dube, P., Hall, J.L., 1999. Ultrasensitive frequency-modulation spectroscopy enhanced by a high-finesse optical cavity: theory and application to overtone transitions of C_2H_2 and C_2HD. J. Opt. Soc. Am. B 16, 2255–2268.

Maithani, S., Mandal, S., Maity, A., Pal, M., Pradhan, M., 2018. High-resolution spectral analysis of ammonia near 6.2 μm using a cw EC-QCL coupled with cavity ring-down spectroscopy. Analyst 143, 2109–2114.

Maity, A., Pal, M., Banik, G.D., Maithani, S., Pradhan, M., 2017. Cavity ring-down spectroscopy using an EC-QCL operating at 7.5 μm for direct monitoring of methane isotopes in air. Laser Phys. Lett. 14, 115701.

McHale, L.E., Hecobian, A., Yalin, A.P., 2016. Open-path cavity ring-down spectroscopy for trace gas measurements in ambient air. Opt. Expr. 24, 5523.

Medina, D.S., Liu, Y., Wang, L., Zhang, J., 2011. Detection of sulfur dioxide by cavity ring-down spectroscopy. Environ. Sci. Techno. 45, 1926–1931.

Min, K.E., Washenfelder, R.A., Dubé, W.P., Langford, A.O., Edwards, P.M., Zarzana, K.J., Stutz, J., Lu, K., Rohrer, F., Zhang, Y., Brown, S.S., 2016. A broadband cavity enhanced absorption spectrometer for aircraft measurements of glyoxal, methylglyoxal, nitrous acid, nitrogen dioxide, and water vapor. Atmos. Meas. Tech. 9, 423–440.

Morville, J., Romanini, D., Kachanov, A.A., Chenevier, M., 2004. Two schemes for trace detection using cavity ringdown spectroscopy. Appl. Phys. B 78, 465–476.

Nwaboh, J.A., Persijn, S., Heinrich, K., Sowa, M., Hering, P., Werhahn, O., 2012. QCLAS and CRDS-based CO quantification as aimed at in breath measurements. Int. J. Spectrosc. 1–10, 2012.

Odame-Ankrah, C.A., Osthoff, H.D., 2011. A compact diode laser cavity ring-down spectrometer for atmospheric measurements of NO_3 and N_2O_5 with automated zeroing and calibration. Appl. Spectrosc. 65, 1260–1268.

O'Keefe, A., Deacon, D.A., 1988. Cavity ring-down optical spectrometer for absorption measurements using pulsed laser sources. Rev. Sci. Instrum. 59, 2544–2551.

Orr, B.J., He, Y., 2011. Rapidly swept continuous-wave cavity-ringdown spectroscopy. Chem. Phys. Lett. 512, 1–20.

Osthoff, H.D., Brown, S.S., Ryerson, T.B., Fortin, T.J., Lerner, B.M., Williams, E.J., Pettersson, A., Baynard, T., Dubé, W.P., Ciciora, S.J., Ravishankara, A.R., 2006. Measurement of atmospheric NO_2 by pulsed cavity ring-down spectroscopy. J. Geophys. Res. Atm. 111, 1–10.

Paldus, B.A., Harb, C.C., Spence, T.G., Wilke, B., Xie, J., Harris, J.S., Zare, R.N., 1998. Cavity-locked ring-down spectroscopy. J. Appl. Phys. 83, 3991–3997.

Paldus, B.A., Kachanov, A.A., 2005. An historical overview of cavity-enhanced methods. Can. J. Phys. 83, 975–999.

Pan, H., Cheng, C.F., Sun, Y.R., Gao, B., Liu, A.W., Hu, S.M., 2011. Laser-locked, continuously tunable high resolution cavity ring-down spectrometer. Rev. Sci. Instrum. 82, 103110.

Park, J., Nam, G.J., Tokmakov, I.V., Lin, M.C., 2006. Experimental and theoretical studies of the phenyl radical reaction with propene. J. Phys. Chem. A 110, 8729–8735.

Parkes, A.M., Fawcett, B.L., Austin, R.E., Nakamichi, S., Shallcross, D.E., Orr-Ewing, A.J., 2003. Trace detection of volatile organic compounds by diode laser cavity ring-down spectroscopy. Analyst 128, 960–965.

Parkes, A.M., Lindley, R.E., Orr-Ewing, A.J., 2004. Combining preconcentration of air samples with cavity ring-down spectroscopy for detection of trace volatile organic compounds in the atmosphere. Anal. Chem. 76, 7329–7335.

Pradhan, M., Lindley, R.E., Grilli, R., White, I.R., Martin, D., Orr-Ewing, A.J., 2008. Trace detection of C_2H_2 in ambient air using continuous wave cavity ring-down spectroscopy combined with sample pre-concentration. Appl. Phys. B 90, 1–9.

Romanini, D., Gambogi, J., Lehmann, K.K., 1995. Cavity ring-down spectroscopy with CW diode laser excitation. In: Proceedings of 50th International Symposium on Molecular Spectroscopy, Columbus OH.

Romanini, D., Kachanov, A., Sadeghi, N., 1997a. CW cavity ring down spectroscopy. Chem. Phys. Lett. 264, 316–322.

Romanini, D., Kachanov, A.A., Stoeckel, F., 1997b. Cavity ringdown spectroscopy: broad band absolute absorption measurements. Chem. Phys. Lett. 270, 546–550.

Romanini, D., Kachanov, A.A., Stoeckel, F., 1997c. Diode laser cavity ring down spectroscopy. Chem. Phys. Lett. 270, 538–545.

Sadiek, I., Shi, Q., Wallace, D.W., Friedrichs, G., 2017. Quantitative mid-infrared cavity ringdown detection of methyl iodide for monitoring applications. Anal. Chem. 89, 8445–8452.

Schmidt, F.M., Vaittinen, O., Metsälä, M., Kraus, P., Halonen, L., 2010. Direct detection of acetylene in air by continuous wave cavity ring-down spectroscopy. Appl. Phys. B 101, 671–682.

Schulz, K.J., Simpson, W.R., 1998. Frequency-matched cavity ring-down spectroscopy. Chem. Phys. Lett. 297, 523–529.

Spence, T.G., Harb, C.C., Paldus, B.A., Zare, R.N., Willke, B., Byer, R.L., 2000. A laser-locked cavity ring-down spectrometer employing an analog detection scheme. Rev. Sci. Instrum. 71, 347–353.

Srivastava, N., Wang, C., 2011. Determination of OH radicals in an atmospheric pressure helium microwave plasma jet. IEEE Trans. Plasma Sci. 39, 918–924.

Stacewicz, T., Wojtas, J., Bielecki, Z., Nowakowski, M., Mikołajczyk, J., Mędrzycki, R., Rutecka, B., 2012. Cavity ring down spectroscopy: detection of trace amounts of substance. Opto-Electron. Rev. 20, 53–60.

Taha, Y.M., Odame-Ankrah, C.A., Osthoff, H.D., 2013. Real-time vapor detection of nitroaromatic explosives by catalytic thermal dissociation blue diode laser cavity ring-down spectroscopy. Chem. Phys. Lett. 582, 15–20.

Thieser, J., Schuster, G., Schuladen, J., Phillips, G.J., Reiffs, A., Parchatka, U., Pöhler, D., Lelieveld, J., Crowley, J.N., 2016. A two-channel thermal dissociation cavity ring-down spectrometer for the detection of ambient NO_2, RO_2NO_2 and $RONO_2$. Atmos. Meas. Tech. 9, 553–576.

Tonokura, K., Koshi, M., 2003. Cavity ring-down spectroscopy of the benzyl radical. J. Phys. Chem. A 107, 4457–4461.

Truong, G.W., Anstie, J.D., May, E.F., Stace, T.M., Luiten, A.N., 2015. Accurate lineshape spectroscopy and the Boltzmann constant. Nat. Commun. 6, 8345.

Vaittinen, O., Manfred Schmidt, F., Metsala, M., Halonen, L., 2013. Exhaled breath biomonitoring using laser spectroscopy. Curr. Anal. Chem. 9, 463–475.

Venables, D.S., Gherman, T., Orphal, J., Wenger, J.C., Ruth, A.A., 2006. High sensitivity in situ monitoring of NO_3 in an atmospheric simulation chamber using incoherent broadband cavity-enhanced absorption spectroscopy. Environ. Sci. Techno. 40, 6758–6763.

Ventrillard-Courtillot, I., Sciamma O'Brien, E., Kassi, S., Méjean, G., Romanini, D., 2010. Incoherent broad-band cavity-enhanced absorption spectroscopy for simultaneous trace measurements of NO_2 and NO_3 with a LED source. Appl. Phys. B 101, 661–669.

Wada, R., Beames, J.M., Orr-Ewing, A.J., 2007. Measurement of IO radical concentrations in the marine boundary layer using a cavity ring-down spectrometer. J. Atmos. Chem. 58, 69–87.

Wada, R., Orr-Ewing, A.J., 2005. Continuous wave cavity ring-down spectroscopy measurement of NO_2 mixing ratios in ambient air. Analyst 130, 1595–1600.

Wagner, N.L., Dubé, W.P., Washenfelder, R.A., Young, C.J., Pollack, I.B., Ryerson, T.B., Brown, S.S., 2011. Diode laser-based cavity ring-down instrument for NO_3, N_2O_5, NO, NO_2 and O_3 from aircraft. Atm. Sci. Tech. 4, 1227–1240.

Wang, C., Sahay, P., 2009. Breath analysis using laser spectroscopic techniques: breath biomarkers, spectral fingerprints, and detection limits. Sensors 9, 8230–8262.

Wang, C., Srivastava, N., Jones, B.A., Reese, R.B., 2008. A novel multiple species ringdown spectrometer for in situ measurements of methane, carbon dioxide, and carbon isotope. Appl. Phys. B 92, 259–270.

Wang, C., Surampudi, A.B., 2008. An acetone breath analyzer using cavity ringdown spectroscopy: an initial test with human subjects under various situations. Meas. Sci. Technol. 19, 105604.

Wang, J., Sun, Y.R., Tao, L.G., Liu, A.W., Hu, S.M., 2017a. Communication: molecular near-infrared transitions determined with sub-kHz accuracy. J. Chem. Phys. 147, 091103.

Wang, J., Sun, Y.R., Tao, L.G., Liu, A.W., Hua, T.P., Meng, F., Hu, S.M., 2017b. Comb-locked cavity ring-down saturation spectroscopy. Rev. Sci. Instrum. 88, 043108.

Wang, J., Yu, J., Mo, Z., He, J., Dai, S., Meng, J., Liu, Y., Zhang, X., Yi, H., 2019. Multicomponent gas detection based on concise CW-cavity ring-down spectroscopy with a bow-tie design. Appl. Opt. 58, 2773.

Wang, Z., Sun, M., Wang, C., 2016. Detection of melanoma cancer biomarker dimethyl disulfide using cavity ringdown spectroscopy at 266 nm. Appl. Spectrosc. 70, 1080–1085.

Washenfelder, R.A., Wagner, N.L., Dube, W.P., Brown, S.S., 2011. Measurement of atmospheric ozone by cavity ring-down spectroscopy. Environ. Sci. Techno. 45, 2938–2944.

Werle, P., 2011. Accuracy and precision of laser spectrometers for trace gas sensing in the presence of optical fringes and atmospheric turbulence. Appl. Phys. B 102, 313–329.

Wheeler, M.D., Newman, S.M., Ishiwata, T., Kawasaki, M., Orr-ewing, A.J., 1998. Cavity ring-down spectroscopy of the $A^2\Pi_{3/2}$ $X^2\Pi_{3/2}$ transition of BrO. Chem. Phys. Lett. 285, 346–351.

Wojtas, J., Bielecki, Z., 2008. Signal processing system in cavity enhanced spectroscopy. Opto-Electron. Rev. 16, 420–427.

Wojtas, J., Mikolajczyk, J., Bielecki, Z., 2013. Aspects of the application of cavity enhanced spectroscopy to nitrogen oxides detection. Sensors 13, 7570–7598.

Zalicki, P., Zare, R.N., 1995. Cavity ring-down spectroscopy for quantitative absorption measurements. J. Chem. Phys. 102, 2708–2717.